

Article

## DEEP LEARNING-BASED DETECTION OF GRAPEVINE FANLEAF VIRUS IN TÜRKİYE: A COMPARATIVE STUDY OF ROBOFLOW 3.0, YOLO-NAS, YOLOV11, AND YOLOV12

### DETECÇÃO DO GRAPEVINE FANLEAF VIRUS NA TURQUIA BASEADA EM APRENDIZAGEM APROFUNDADA: UM ESTUDO COMPARATIVO DE ROBOFLOW 3.0, YOLO-NAS, YOLOV11 E YOLOV12

Lerzan Öztürk<sup>1</sup>, Bahadır Şin<sup>2\*</sup><sup>1</sup>Independent Researcher, 59200, Süleymanpaşa, Tekirdağ, Türkiye.<sup>2</sup>Plant Protection Department, Faculty of Agriculture, Sakarya University of Applied Science, 54050, Sakarya, Türkiye.

\* Corresponding author: Tel.: +905053063638; e-mail: sinbahadir@gmail.com

(Received 16.06.2025. Accepted 23.03.2026)

#### SUMMARY

Grapevine fanleaf virus (GFLV) poses a significant phytopathological threat to global viticulture, demanding the development of rapid and accurate detection methodologies to mitigate economic losses. In this study, four deep learning-based object detection architectures were implemented and comparatively evaluated, ROBOFLOW 3.0 (Fast), YOLO-NAS (Accurate and Medium), YOLOv11 (Fast), and the latest YOLOv12 (Fast), for the automated identification of GFLV symptoms on grapevine leaves. A custom dataset comprising high-resolution images captured under diverse vineyard conditions was curated and meticulously annotated. YOLO models were trained on 100-350 epochs. Model performance was assessed using metrics such as Precision, Recall, Mean average precision at Intersection over Union (IoU)=0.5 (mAP@50), Mean average precision across IoU thresholds (mAP@50–95), and F1 score. Among the evaluated models, YOLOv11 Fast achieved the highest mAP@50 value (93.4%) and an F1 score of 88.3%. In comparison, ROBOFLOW 3.0 Fast reached a mAP@50 of 89.4% and an F1 score of 86%, YOLO-NAS Accurate achieved mAP@50 92.4% and F1 85.2%, and YOLO-NAS Medium obtained 91.9% and 85.3%, respectively. The latest version YOLOv12 Fast yielded mAP@50 91.3% and F1 86.5%. These results highlight the potential of next-generation YOLO architectures for high-throughput, real-time GFLV detection, offering a scalable and efficient solution for precision viticulture and integrated disease management.

#### RESUMO

O Vírus do urticado da videira (*Grapevine fanleaf virus* - GFLV) representa uma ameaça fitopatológica significativa para a viticultura global, exigindo o desenvolvimento de metodologias de detecção rápidas e precisas a fim de mitigar perdas econômicas. Neste estudo, foram implementados e avaliados comparativamente quatro modelos de detecção de objetos baseados em aprendizagem aprofundada: ROBOFLOW 3.0 (Fast), YOLO-NAS (Accurate and Medium), YOLOv11 (Fast) e o mais recente YOLOv12 (Fast), para a identificação automatizada de sintomas de GFLV em folhas de videira. Foi elaborado um conjunto de dados personalizado, composto por imagens de alta resolução captadas sob diversas condições em vinhedos, com anotações detalhadas. Os modelos YOLO foram treinados considerando 100 a 350 épocas. O desempenho dos modelos foi avaliado através de métricas como precisão, revocação (recall), média de precisão média para Intersection over Union (IoU)=0.5 (mAP@50), média de precisão média para múltiplos limiares de IoU (mAP@50–95) e F1 score. Entre os modelos avaliados, o YOLOv11 Fast alcançou o maior valor de mAP@50 (93,4%) e um F1 score de 88,3%. Em comparação, o ROBOFLOW 3.0 Fast atingiu um mAP@50 de 89,4% e um F1 score de 86%, enquanto o YOLO-NAS Accurate alcançou um mAP de 92,4% e F1 de 85,2%, e o YOLO-NAS Medium obteve 91,9% e 85,3%, respetivamente. A versão mais recente, YOLOv12 Fast, apresentou um mAP@50 de 91,3% e um F1 score de 86,5%. Esses resultados destacam o potencial das arquiteturas YOLO de nova geração para a detecção de GFLV em tempo real e em larga escala, oferecendo uma solução escalável e eficiente para a viticultura de precisão e o manejo integrado de doenças.

**Keywords:** Grapevine virus detection, image processing, deep learning, *Nepovirus*, precision viticulture.**Palavras-chave:** Detecção de vírus da videira, processamento de imagem, aprendizagem automática, *Nepovirus*, viticultura de precisão.

© Öztürk and Şin, 2025.

This is an Open Access article distributed under the terms of the Creative Commons Attribution License

<https://creativecommons.org/licenses/by/4.0>, which permits unrestricted use, distribution, and reproduction in any medium, provided the original work is properly cited

## INTRODUCTION

Viticulture represents one of the most economically and culturally important agricultural sectors globally, serving a vital function in fruit production and the wine industry (Maroun *et al.*, 2017). Virus diseases affecting grapevines pose serious threats to the sustainability of viticulture by causing yield losses, quality deterioration, and substantial economic damage. Among these diseases, Grapevine fanleaf virus (GFLV), belonging to the genus *Nepovirus*, stands out as one of the most destructive pathogens (Banora *et al.*, 2022; Fajardo *et al.*, 2023). GFLV induces symptoms such as growth abnormalities, leaf deformation, leaf color changes, significant reductions in fruit quality, and reduced rooting and grafting performance (Jackson, 2014). GFLV is the most prevalent grapevine virus in Türkiye, with reported incidence rates ranging from 10.7% to 57% across various regions (Çiğsar *et al.*, 2002; Öztürk *et al.*, 2017). The virus is vectored by the nematode *Xiphinema index*, which acquires the virus after feeding on infected grapevine roots and subsequently transmits it to healthy plants. A nematode can become viruliferous after a single feeding event and can retain its ability to transmit the virus for four to eight weeks while feeding on host plants (Taylor and Raski, 1964; M'rabet Samaali *et al.*, 2022). Effective virus transmission can occur within 5-15 min at soil temperatures between 13-24 °C (Van Zyl *et al.*, 2012). GFLV can persist in *X. index* for up to eight months without feeding on host plants (Raski and Hewitt, 1960; Raski *et al.*, 1965; Demangeat *et al.*, 2005).

Methods for GFLV detection rely largely on the visual observation of disease symptoms and subsequent serological and molecular laboratory-based assays, such as ELISA (Enzyme-Linked ImmunoSorbent Assay) and RT-PCR (Real-Time PCR) (Rowhani *et al.*, 1993). Although these methods can provide accurate results, they are often labor-intensive, time-consuming, costly, and operationally challenging, particularly when applied to a high number of samples (Singh and Misra, 2017). Consequently, there is a growing need in plant pathology for methods that are rapid, cost-effective, and user-friendly, enabling timely and accurate identification of pathogens and pests under field and laboratory conditions, as these organisms pose a constant risk to healthy plants (Rahman *et al.*, 2023).

In recent years, advancements in artificial intelligence (AI) and deep learning-based image processing technologies have opened new approaches for the automated diagnosis of plant diseases (Jafar *et al.*, 2024). Convolutional neural networks (CNNs) have emerged as the leading approach for this task due to their strong capability to automatically extract, learn, and classify complex visual features from raw image data (Khanam *et al.*, 2024). Among these technologies, the YOLO (You Look Once) object detection architecture has

emerged as a prominent tool for object detection tasks, offering a remarkable balance between inference speed and detection accuracy, making it particularly suitable for real-time agricultural applications (Ghafar *et al.*, 2024). YOLO models divide input images into grids and simultaneously predict bounding boxes and class probabilities, enabling fast detection and classification of multiple objects (Redmon *et al.*, 2016; Ali and Zhang, 2024; Gheorghe *et al.*, 2024).

Recent versions, such as YOLOv11, have introduced significant improvements in computational efficiency and detection precision under variable environmental conditions (Wang *et al.*, 2025). These advancements have further expanded the applicability of YOLO models in agricultural practices, ranging from weed identification to early disease detection and pest monitoring (Liu *et al.*, 2024; Medojevic, 2024; Tripathi *et al.*, 2024; Qi and Wang, 2025; Zhu *et al.*, 2025).

This study aimed to evaluate the effectiveness of YOLO-based deep learning models in detecting symptoms of GFLV on grapevine leaves. For this purpose, a customized dataset consisting of high-resolution images captured both in diverse vineyard environments and under laboratory conditions was developed and meticulously annotated. The vines used for image acquisition were pre-tested using serological methods, and only those confirmed to be GFLV-positive were selected. Additionally, images of vines infected with viruses other than GFLV and virus-free (healthy) vines were included in the dataset. The evaluated model variants included YOLOv11 (Fast), YOLOv12 (Fast), YOLO-NAS (Accurate and Medium), and the proprietary ROBOFLOW 3.0 (Fast) trained within the ROBOFLOW platform. Model performance was evaluated using standard metrics including Precision, Recall, Mean average precision at an IoU threshold of 0.5 (mAP@50), mean average precision across IoU thresholds (mAP@50-95), and F1 score, respectively.

## MATERIALS AND METHODS

### GFLV Image Dataset Preparation

Over a three-year period, beginning in 2022, a comprehensive field study was conducted in vineyards across the Süleymanpaşa District of Tekirdağ Province (Figure 1A), located in the Thrace region of Türkiye, to assess the distribution of Grapevine fanleaf virus (GFLV). Surveys were conducted during the active vegetative growth period (May–July), when foliar symptoms of GFLV are most clearly expressed under field conditions. Grapevines displaying suspected viral symptoms were examined for typical signs of GFLV, including mosaic patterns, leaf deformation, chlorosis, vein clearing, vein banding, and reduced growth.

Leaf samples were collected mainly from the middle and lower parts of the canopy, especially from shoots where symptoms were clearly observed. In total, 53 vineyards were surveyed. All symptomatic samples were analyzed for the presence of GFLV by DAS-ELISA (Double Antibody Sandwich ELISA) and Polymerase Chain Reaction (PCR) assays. DAS-ELISA tests were conducted using commercially available GFLV-specific antibody kits (BIOREBA) in accordance with the manufacturer's protocol. For molecular detection, total RNA was isolated using a silica column-based extraction kit, and complementary DNA (cDNA) was synthesized with oligo(dT) primers. PCR amplification was performed using the GFLV-specific primer pair reported by Gambino and Gribaudo (2006), consisting of the forward primer GFLV-F (5'-TGCTGGATATCGTGACCCTGT-3') and the reverse primer GFLV-R (5'-AAGGTATGCCTGCTTCAGTGG-3'), generating a 118 bp amplicon. Based on the combined serological and molecular analyses, GFLV infection was confirmed in 27 vineyards established with varieties such as 'Merlot', 'Muscat of Hamburg', 'Chardonnay' and 'Pinot Noir'. In ELISA assays, absorbance values at 405 nm for positive samples ranged between 1155-4500 (Positive control: 3.365; Negative control: 0.076). PCR results consistently produced 118 bp bands corresponding to the expected fragment size.

Upon confirmation, high-resolution RGB (Red, Green, and Blue) images (6000 × 4000 pixels) were captured using a 48-megapixel Nikon (Nikon Corporation, Tokyo, Japan) digital camera under both natural field conditions and laboratory settings. Field images were captured under natural vineyard conditions, including variable lighting, background complexity, and canopy structure, whereas laboratory images were captured under controlled lighting and background conditions to minimize environmental variability and enhance feature clarity. Imaging focused on symptomatic leaves with clearly visible signs of infection. To ensure the diagnostic value and diversity of the dataset, only high-quality images displaying distinct symptoms were retained. The final dataset consisted of 961 images: 946 depicting symptomatic tissues (GFLV-only, 728 images; GFLV co-infected with other viruses, 203 images; and GFLV-infected tissues with partially healthy appearance, 15 images), and 15 showing asymptomatic healthy leaves (Figure 1B). Asymptomatic (healthy) leaves included in the dataset were tested by DAS-ELISA and PCR and confirmed to be virus-free (Absorbance values: 0.007-0.076). All images were resized to 640 × 640 pixels to conform to convolutional neural network input requirements. The dataset was randomly divided into three subsets: 70% for training, 20% for validation, and 10% for testing. This balanced distribution provided a robust foundation for developing and evaluating deep learning models aimed at automated GFLV symptom detection.

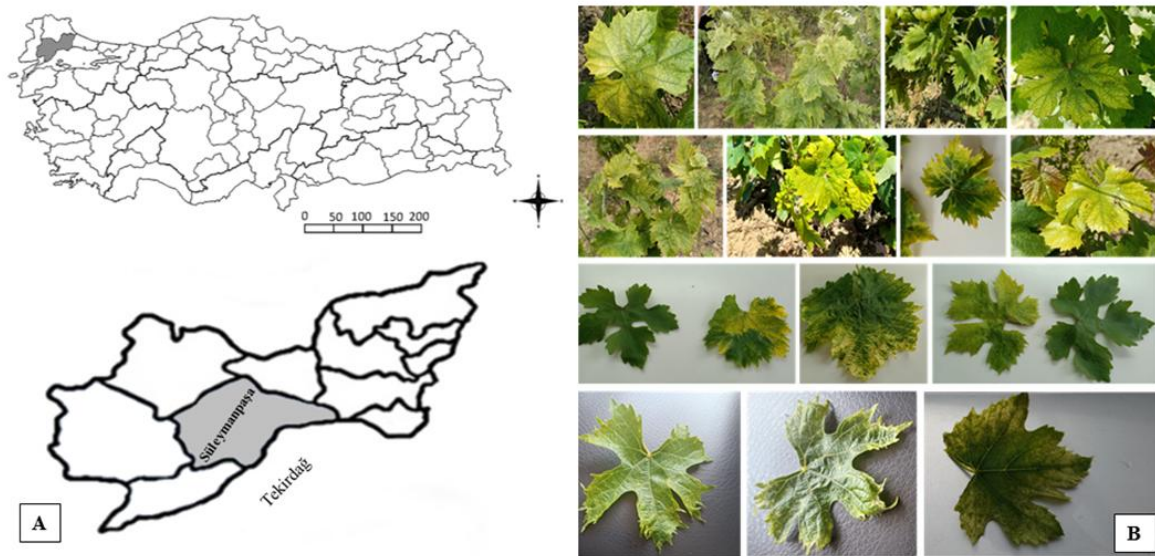


**Figure 1.** A) Study area map; B) Representative images of grapevine leaves exhibiting Grapevine fanleaf virus symptoms used in the annotated dataset.

Each image was annotated using the MakeSense labeling tool and a total number of 1.192 annotations was generated. This labeled dataset served as the

primary resource for training YOLO-based object detection models. Image processing and testing were performed using Ultralytics' PyTorch-based

framework. The trained models included ROBOFLOW 3.0 Fast (compatible with YOLOv8), YOLOv11 (Fast), YOLOv12 (Fast) and YOLO-NAS (Accurate and Medium) models developed by Deci.ai, and implemented via the ROBOFLOW platform (Brucal *et al.*, 2024) (Figure 2).

Training was performed using stochastic gradient descent (SGD) optimizer with a learning rate of

0.001, momentum of 0.937, and weight decay of 0.0005. A warm-up phase of 3 epochs was applied, and training was conducted over 100 epochs with a batch size ranging from 8 to 16. Input image size was set to  $640 \times 640$  pixels for all models.

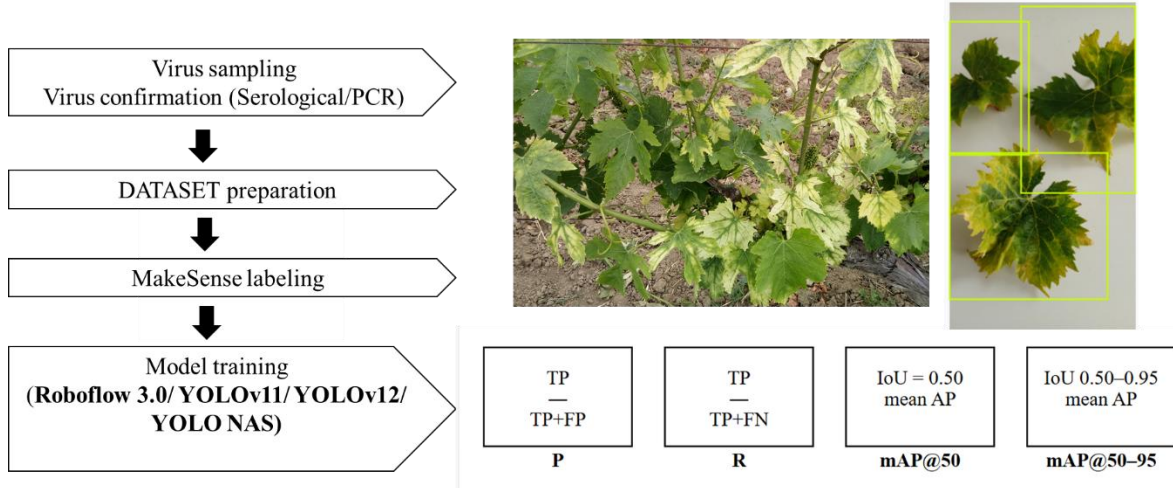


**Figure 2.** Schematic representation of the YOLO training workflow and detection outputs from ROBOFLOW 3.0, YOLOv11, YOLOv12 and YOLO-NAS models trained on a Grapevine fanleaf virus (GFLV) dataset.

### YOLO Model Performance Evaluation

Following training, each model underwent a validation phase, and performance was evaluated using standard object detection metrics, including Precision (Equation 1), Recall (Equation 2), Mean average precision (mAP) and mAP@50-95 (Equation 3), and F1 score (Equation 4). Training spanned between 100-350 epochs depending on the model, with continuous monitoring of core loss functions such as box loss (box\_loss), distribution focal loss (dfl\_loss), and classification loss (cls\_loss). Training graphs (loss curves, mAP trends) and model outputs (e.g., confusion matrix, F1 score) were also reviewed in detail.

To evaluate the detection performance of the model, standard classification outcomes were defined. A false positive (FP) was considered as a case where a region without GFLV symptoms was incorrectly identified as infected. A false negative (FN) referred to instances in which visible GFLV symptoms present in the annotated ground truth were not detected by the model.

Using these outcomes, several performance metrics were calculated. Precision (P) expressed the proportion of correctly identified GFLV-positive detections among all predicted positives. The F1

score, calculated as the harmonic mean of precision and recall, was used to provide a balanced assessment of model performance, particularly in cases in which relying solely on accuracy might be misleading. In addition, mean Average Precision (mAP) was determined from the area under the Precision–Recall (PR) curve. Since the study focused on a single-class detection task, the mAP value directly reflected the model’s ability to distinguish GFLV symptoms across different confidence thresholds.

$$P = TP / (TP+FP) \quad \text{Eq.1}$$

$$\text{Recall (R)} = TP / (TP+FN) \quad \text{Eq.2}$$

$$mAP = \frac{1}{N} \sum_i^N AP_i \quad \text{Eq.3}$$

N: Number of object classes

AP<sub>i</sub>: Average Precision for class i

$$F1 = 2 \times [(Precision \times Recall) / (Precision + Recall)] \quad \text{Eq.4}$$

## RESULTS AND DISCUSSION

Five YOLO variants were evaluated on the annotated grapevine leaf dataset, and all models demonstrated high performance in detecting Grapevine fanleaf virus (GFLV) symptoms (Table I). The YOLOv11

Fast achieved the highest overall detection performance among the tested architectures. YOLOv12 Fast and both YOLO-NAS variants also exhibited strong and competitive results, while ROBOFLOW 3.0 Fast showed comparatively lower performance levels.

**Table I**

Overall comparative performance metrics of trained YOLO models

Model	Variant	mAP@50 (%)	Precision (%)	Recall (%)	F1 (%)
ROBOFLOW 3.0	Fast	89.4	88.3	83.8	86
YOLOv11	Fast	93.4	90.1	86.5	88.3
YOLOv12	Fast	91.3	88.2	84.8	86.5
YOLO-NAS	Accurate	92.4	82.5	88.2	85.2
	Medium	91.9	83.4	87.3	85.3

All models achieved precision, recall, and mAP@50 values exceeding 80%, confirming the feasibility of image-based GFLV recognition under natural field conditions. None of the models reached 100% accuracy, which is consistent with the inherent biological variability of GFLV symptoms. Chlorosis, mosaic patterns, vein banding, and leaf deformation may visually overlap with nutrient deficiencies, water stress, herbicide injury, or other viral infections, resulting in unavoidable classification ambiguity in complex vineyard environments. Additionally, in certain vineyards, higher weed density, particularly of *Sinapis arvensis* and *Sorghum halepense*, increased background complexity, which may have contributed to lower detection confidence under heterogeneous field conditions.

Findings of this study were consistent with several other studies. Similar to GFLV detection, YOLOv11 has shown high diagnostic accuracy across multiple crops. It has been successfully applied to detect foliar diseases such as leaf blight and rust in apple, maize, and potato (Abid *et al.*, 2024; Aldakheel *et al.*, 2024; Medojević, 2024; Al Husaini *et al.*, 2025; Lee *et al.*, 2025; Gao *et al.*, 2025; Tao *et al.*, 2025; Temrokov and Bzhikhatlov, 2025), demonstrating strong generalization capacity across heterogeneous agricultural environments. Similarly, YOLOv8 achieved 99% precision, 98.9% mAP, and 91.9% recall for detecting bacterial spot, black spot, early and late blight, and leaf mold detection in tomato

(Brucal *et al.*, 2024). YOLO-NAS has also been applied to weed detection and disease recognition, including wilt detection and other plant protection tasks (Slimani *et al.*, 2023; Patel *et al.*, 2024; Sonawane and Patil, 2024; Mora *et al.*, 2025).

The comparative evaluation of ROBOFLOW 3.0 Fast, YOLOv11 Fast, YOLOv12 Fast, YOLO-NAS Accurate, and YOLO-NAS Medium models revealed consistent learning behavior and stable convergence patterns across all architectures for the detection of Grapevine fanleaf virus (GFLV) symptoms.

The ROBOFLOW 3.0 Fast model, trained for 50 epochs, exhibited stable and progressive learning dynamics. Training losses, including box loss, classification loss (cls\_loss), and distribution focal loss (dfl\_loss), decreased steadily throughout training. Box loss declined from approximately 1.5 to 1.0, while classification loss decreased markedly from above 2.0 to approximately 0.7, indicating improved localization and classification capabilities. Performance metrics increased rapidly during the early epochs, with precision and recall stabilizing near 0.85. Although slight fluctuations were observed in validation loss components, particularly val/dfl\_loss and val/cls\_loss, no pronounced signs of overfitting were detected (Figure 3). The relatively shorter training duration enabled rapid convergence with stable generalization performance.

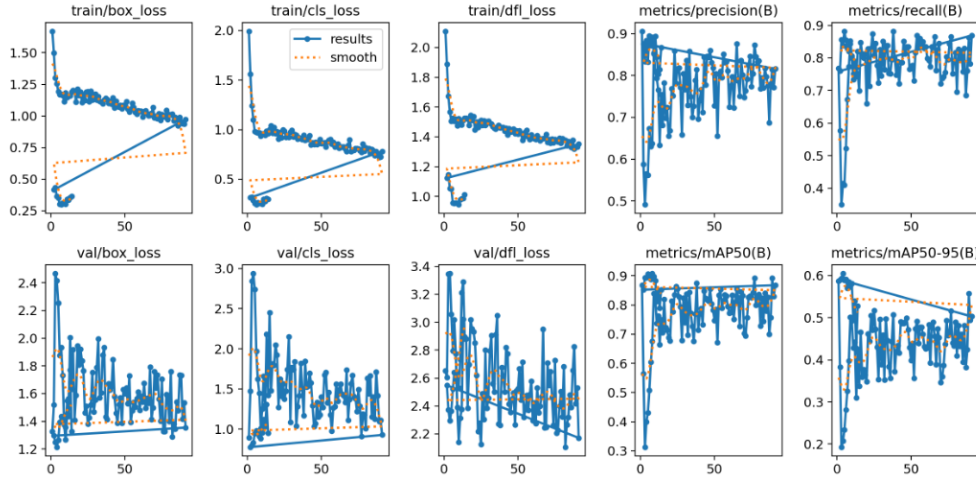


**Figure 3.** ROBOFLOW 3.0 Fast (compatible with YOLOv8) training curves: Loss functions and performance metrics. The plots illustrate the progression of box\_loss, cls\_loss, and dfl\_loss, together with precision, recall, mAP@50, and mAP@50-95 metrics. The x-axis represents training epochs, and the y-axis corresponds to loss values or performance scores.

In contrast, YOLOv11 Fast, trained for 200 epochs, showed a steady optimization process across all loss components. Box loss decreased from around 1.8 in the initial epochs to below 1.0 by the end of training. Classification loss declined from above 3.0 to under 1.0, while distribution focal loss decreased from nearly 2.0 to 1.3. Although validation losses displayed sharp fluctuations during the early epochs, they quickly stabilized and followed a downward trend similar to the training losses. After the initial

phase, validation curves remained relatively stable, indicating no clear signs of overfitting. Performance metrics improved consistently throughout training. Precision and recall both exceeded 0.80 in the later epochs, approaching 0.85. The mAP@50 value increased steadily and reached nearly 0.90, while mAP@50-95 improved to around 0.55 before leveling off. Most performance gains occurred within the first 120–150 epochs, after which the curves showed minor incremental improvements (Figure 4).

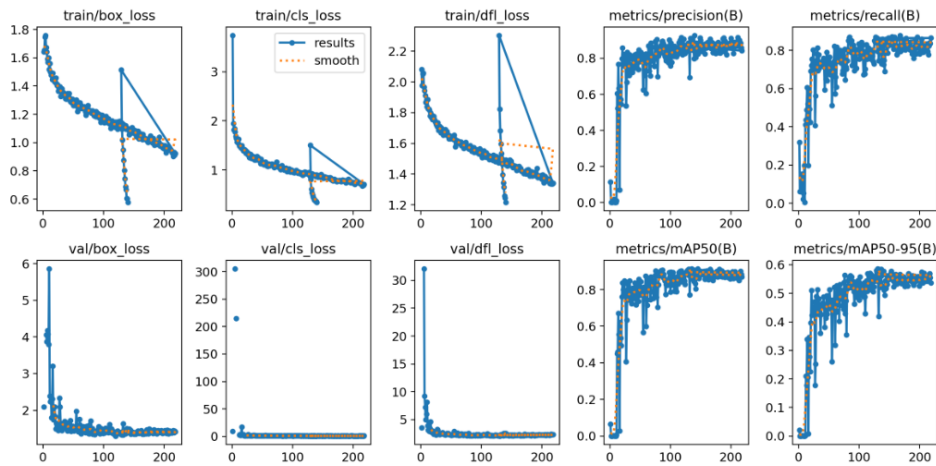


**Figure 4.** YOLOv11 Fast training curves: Loss functions and performance metrics. The plots illustrate the progression of box\_loss, cls\_loss, and dfl\_loss, together with precision, recall, mAP@50, and mAP@50-95 metrics. The x-axis represents training epochs, and the y-axis corresponds to loss values or performance scores.

The YOLOv12 Fast model exhibited a stable learning trend over the 200 training epochs. As shown in Figure 5, the training losses gradually

decreased throughout the process. Box loss declined from 1.5 in the initial epochs to 0.7 by the end of training. Similarly, classification loss decreased from

about 2.6 to nearly 0.5, while `df_l_loss` dropped from roughly 1.8 to 1.2. These reductions indicate progressive improvement in both localization and classification performance. Validation losses showed a comparable downward pattern after the initial fluctuations, remaining close to the training losses in later epochs, which suggests that overfitting was limited. Performance metrics improved steadily during training. Precision increased from below 0.20 in the first epochs to 0.88-0.90, while recall reached around 0.85-0.88 toward the final epochs. The

`mAP@50` value rose consistently and approached 0.90, and `mAP@50-95` gradually increased to nearly 0.58-0.60. Most metrics began to stabilize after approximately 140-160 epochs.

The YOLO-NAS Accurate model showed a stable training pattern over approximately 250 epochs. Classification loss gradually decreased from 0.85 to nearly 0.74, while box loss remained stable, fluctuating between 0.45 and 0.52 before stabilizing close to 0.48 in later epochs.

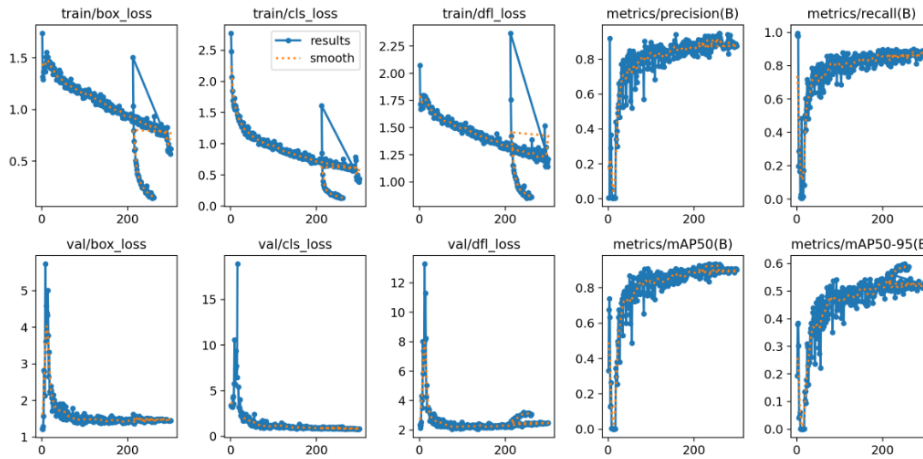


**Figure 5.** YOLOv12 Fast training curves: Loss functions and performance metrics. The plots illustrate the progression of `box_loss`, `cls_loss`, and `df_l_loss`, together with precision, recall, `mAP@50`, and `mAP@50-95` metrics. The x-axis represents training epochs, and the y-axis corresponds to loss values or performance scores.

The object loss showed a slight upward trend during training, increasing from 0.80 to 0.92, but remained within a stable range overall. Precision values fluctuated throughout training, but generally remained between 0.82 and 0.88. Recall demonstrated a gradual upward tendency, approaching 0.88-0.89 in later epochs. The `mAP`

value remained close to 0.90 for most of the training process, while `mAP@50-95` increased slightly over time and stabilized near 0.54-0.56. The model maintained consistent performance across epochs, with limited variation in loss values and stable detection metrics (Figure 6).

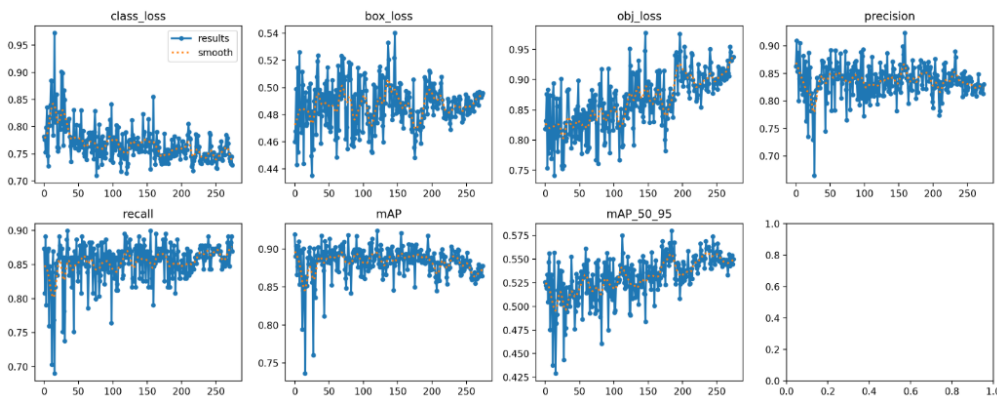


**Figure 6.** YOLO-NAS Accurate training curves: Loss functions and performance metrics. The plots illustrate the progression of `box_loss`, `cls_loss`, and `df_l_loss`, together with precision, recall, `mAP@50`, and `mAP@50-95` metrics. The x-axis represents training epochs, and the y-axis corresponds to loss values or performance scores.

During the training process of the YOLO-NAS Medium model, a rapid optimization phase was observed in the early epochs. The `cls_loss` decreased sharply from 2.8 in the early epochs to below 0.1 within the initial 20-25 epochs, and subsequently stabilized around 0.05 for the remainder of the training. In contrast, `box_loss` showed moderate fluctuations throughout the training process, ranging between approximately 0.40 and 0.52. Despite this variability, the curve remained within a relatively narrow interval and converged near 0.47 in the final epochs.

The `obj_loss` followed a similar pattern, varying between approximately 0.73 and 0.85, before stabilizing close to 0.80 in later epochs. Performance metrics improved rapidly during the early training stage and reached a plateau after approximately 30-40 epochs. Precision stabilized around 0.85, while recall approached 0.86-0.87 in the later epochs. The `mAP@50` value remained close to 0.90-0.91 across most of the training process, and `mAP@50-95` gradually increased and stabilized around 0.54-0.55. The training curves demonstrate a short but effective learning phase without signs of overfitting (Figure 7).

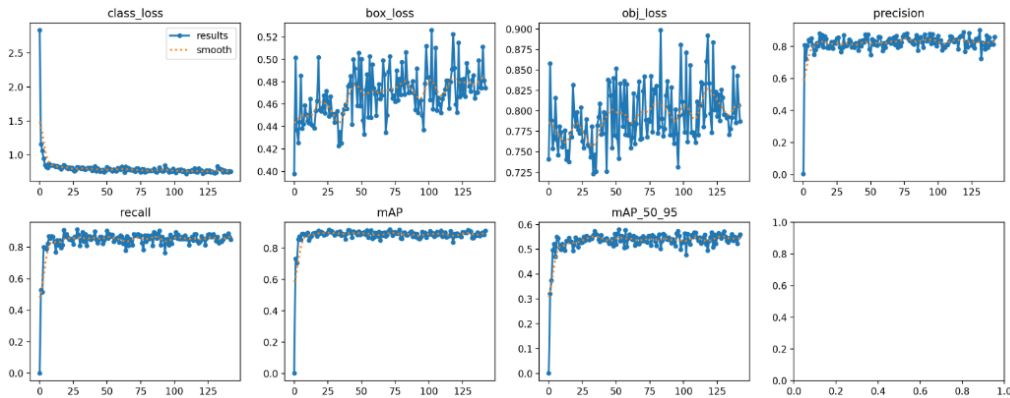


**Figure 7.** YOLO-NAS Medium training curves: Loss functions and performance metrics. The plots illustrate the progression of `box_loss`, `cls_loss`, and `obj_loss`, together with precision, recall, `mAP@50`, and `mAP@50-95` metrics. The x-axis represents training epochs, and the y-axis corresponds to loss values or performance scores.

The confusion matrix findings (Table II) demonstrate noticeable variation in model performance for GFLV detection. ROBOFLOW 3.0 Fast achieved the lowest false positive rate, indicating strong specificity; however, it exhibited a comparatively higher number of missed infected samples, reflecting reduced sensitivity. YOLOv11 Fast improved sensitivity by increasing true positive detections and decreasing false negatives, although this enhancement was associated with a moderate rise in false positives. YOLOv12 Fast showed moderate performance, maintaining a relatively stable balance between detection accuracy and error rate. Among the YOLO-NAS architectures, the Accurate variant achieved the highest sensitivity, identifying the highest number of infected leaves and with the lowest number of missed cases. The YOLO-NAS Medium model demonstrated a more balanced error distribution, combining high detection capability with controlled misclassification levels. Overall, the models exhibited different optimization tendencies, with some prioritizing specificity and others emphasizing detection sensitivity.

The detection task was structured as a single-class object detection problem targeting only GFLV symptoms. Healthy leaves were included in the dataset as background images and were not defined as a separate detection category. For this reason, true

negative (TN) values were not calculated in the conventional binary classification framework, and TN appears as zero in the confusion matrix. The evaluation therefore relies on true positive, false positive, and false negative detections, which is standard practice in single-class object detection studies. Although overall performance levels were comparable, distinct detection tendencies were observed among the models. YOLOv11 Fast achieved the most balanced performance (93.4% `mAP@50`, 90.1% precision, 86.5% recall), maintaining relatively low false negatives while keeping false positives within acceptable limits. YOLO-NAS variants demonstrated higher sensitivity, producing greater true positive detections, but this was accompanied by increased false positive rates, reflecting a trade-off in specificity. YOLOv12 Fast showed strong precision yet generated more false negatives, while ROBOFLOW 3.0 Fast yielded the lowest false positive rate but the highest number of missed infections. From an epidemiological perspective, false negatives are particularly critical, as undetected infected vines may facilitate continued virus dissemination within vineyards. Accordingly, YOLOv11 Fast provided the most balanced and practically applicable performance under field conditions, whereas YOLO-NAS variants may be

advantageous in early infection screening contexts where sensitivity is prioritized.

These performance differences appear to be associated with the architectural priorities and optimization strategies of each model. YOLOv11 integrates efficient feature aggregation and spatial attention mechanisms that promote stable generalization under heterogeneous vineyard conditions (Sapkota *et al.*, 2025). In contrast, YOLOv12 incorporates attention-centric components such as Area Attention (A2) and R-

ELAN; however, the added structural complexity did not result in superior sensitivity under the variable conditions present in field-acquired imagery (Tian *et al.*, 2025). YOLO-NAS models, optimized through neural architecture search, emphasize detection sensitivity but may increase false positive predictions in visually complex plant tissues (Terven *et al.*, 2023). Conversely, ROBOFLOW 3.0 framework exhibited a more conservative detection pattern, consistent with the typical precision–recall trade-off observed in single-stage detection systems.

**Table II**

Confusion matrix results calculated at a fixed confidence threshold (50%) and IoU threshold on the validation+test dataset

Model	Variant	True positive	False negative	False positive	True negative
ROBOFLOW 3.0	Fast	268	69	18	0
YOLOv11	Fast	284	53	31	0
YOLOv12	Fast	273	64	23	0
YOLO-NAS	Accurate	289	48	39	0
YOLO-NAS	Medium	287	50	34	0

Vector-based F1 score distributions (Figure 8) indicated that all evaluated models achieved high detection performance for GFLV symptoms. In all architectures, the majority of test images were concentrated within the higher F1 score interval ( $\geq 0.7$ ). YOLOv12 Fast and YOLO-NAS Accurate exhibited more consistent score distributions, with most samples exceeding F1 values of 0.8. YOLOv11 Fast similarly showed strong clustering in the high-

performance range, although a moderate spread toward intermediate F1 values (0.4–0.7) was observed. ROBOFLOW 3.0 Fast and YOLO-NAS Medium also demonstrated substantial clustering above  $F1 \geq 0.7$ , while a limited number of samples yielded lower F1 scores ( $< 0.4$ ). The F1 score distributions confirm consistent detection performance across models, with variability confined to a minority of test images.

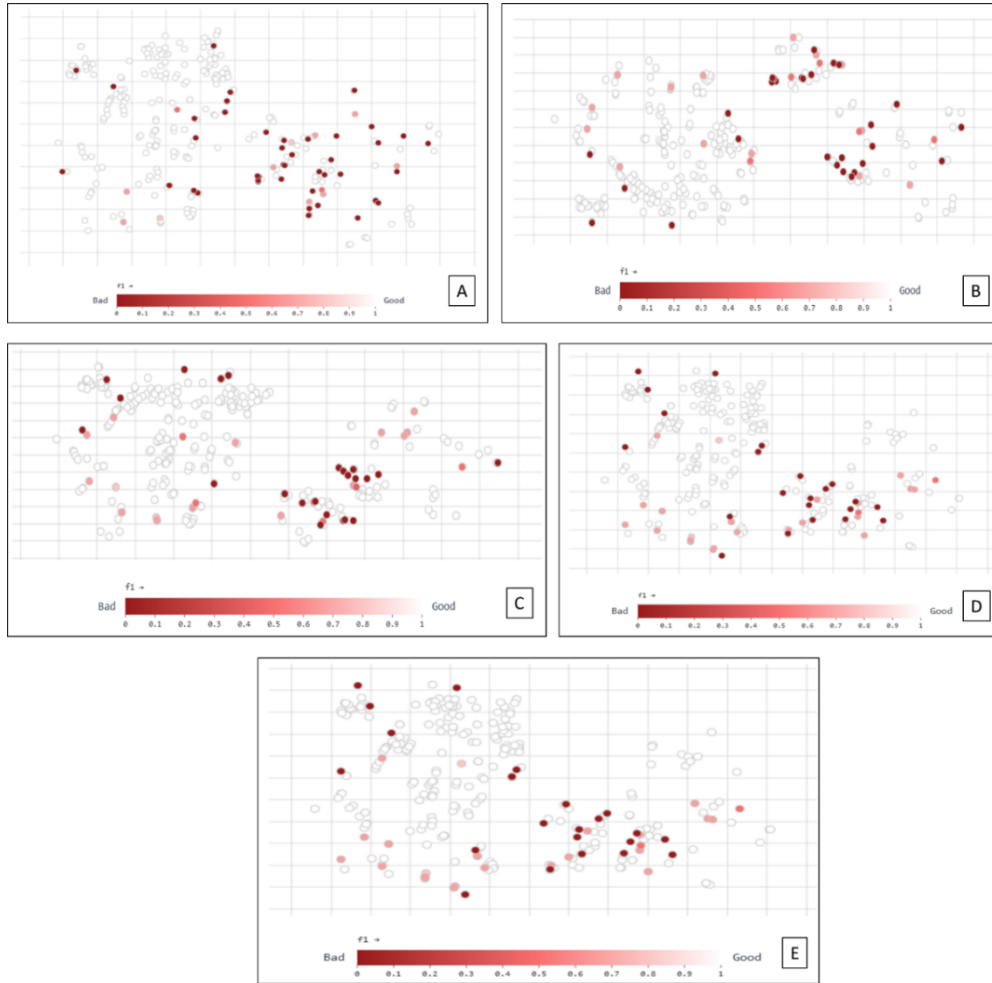


**Figure 8.** Distribution of image-level F1 scores across five YOLO-Based model variants: A) ROBOFLOW 3.0 Fast; B) YOLOv11 Fast; C) YOLOv12 Fast; D) YOLO-NAS Accurate; E) YOLO-NAS Medium. Each point represents a test image, and color intensity reflects the corresponding F1 score (dark red = low performance; light red/white = high performance). The axes reflect the relative distribution of images within the visualization space and do not represent actual spatial coordinates.

The Figure 9 shows representative examples of GFLV detection under both laboratory and field conditions. In the laboratory images (A and C), typical symptoms such as mosaic patterns, vein banding, chlorosis, and leaf deformation were correctly identified, with confidence values between 85% and 90%. In the field images (B and E), despite variations in lighting, background complexity, and

overlapping foliage, the model was able to localize symptomatic leaves with confidence levels ranging from 73% to 83%. These findings indicate that the model maintains stable performance under different environmental conditions. In image D, where clear GFLV symptoms were not observed, no detection was produced, suggesting that the model does not generate excessive false positives.

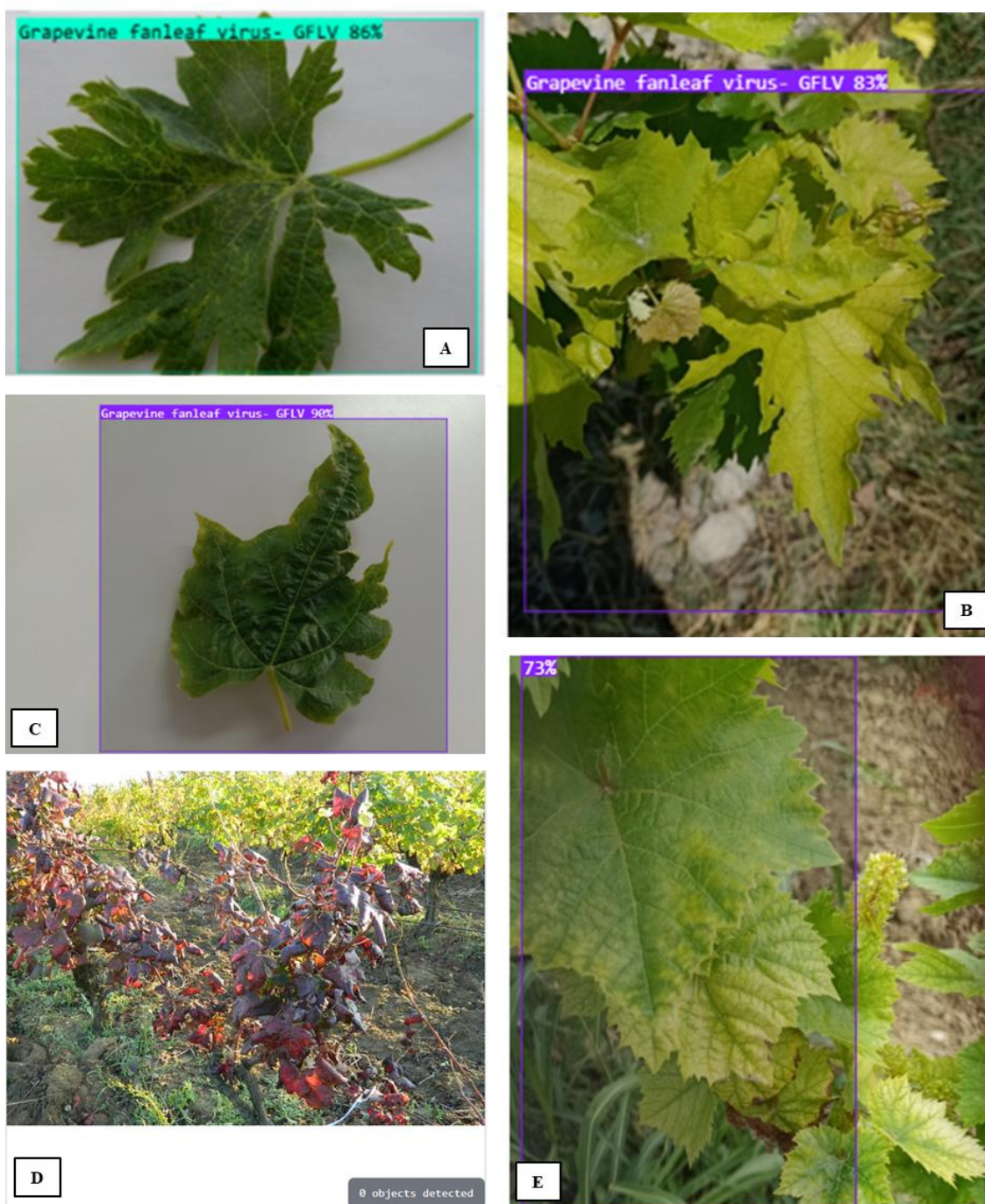


**Figure 9.** Representative detection results of Grapevine fanleaf virus: A) YOLOv 11 Fast; B) YOLO-NAS Accurate; C) ROBOFLOW 3.0 Fast; D) YOLOv12 Fast (Image from Grapevine Leafroll Associated virus infected grapevine. No detection of GFLV); E) YOLO-NAS Accurate .

In this study, the comparison was centered on detection accuracy under vineyard conditions, using precision, recall, and mAP as primary evaluation metrics. Parameters related to computational efficiency, including inference time (ms per image), FPS, and FLOPs, were not evaluated. Since the main objective was to assess model detection capability rather than real-time performance, speed-related benchmarking was beyond the scope of the present work. Future investigations may address this aspect to further evaluate field-level applicability.

Overall, the findings indicate that image-based deep learning models can be successfully applied for GFLV symptom detection under natural vineyard conditions. These systems provide a rapid and non-destructive screening alternative that may support early field-level assessment and management decisions. However, they should be considered complementary tools rather than substitutes for molecular diagnostics such as ELISA or RT-PCR, which remain essential for confirmatory analysis.

Future research should focus on expanding the dataset to include a broader range of abiotic stresses, mixed infections, and symptom variability in order to improve generalization. The incorporation of multispectral imaging approaches may further reduce visual ambiguity and enhance detection reliability under complex vineyard conditions.

## CONCLUSIONS

This study confirms the applicability of deep learning models for detecting Grapevine fanleaf virus (GFLV) symptoms under vineyard conditions. Among the evaluated architectures, YOLOv11 achieved the highest mAP@50 and demonstrated the most balanced overall performance. The results support the potential of YOLO-based models for accurate visual disease detection in precision viticulture. Future studies should expand dataset diversity and explore advanced learning strategies to further improve robustness and reliability.

## CONFLICT OF INTEREST

The authors declare no conflict of interest.

## REFERENCES

- Abid M.S.Z., Jahan B., Al Mamun A., Hossen M.J., Mazumder S.H., 2024. Bangladeshi crops leaf disease detection using YOLOv8. *Heliyon*, **10**, e36694.
- Ali M.L., Zhang Z., 2024. The YOLO framework: A comprehensive review of evolution, applications, and benchmarks in object detection. *Computers*, **13**, 336.
- Aldakheel E.A., Zakariah M., Alabdallal A. H., 2024. Detection and identification of plant leaf diseases using YOLOv4. *Frontiers in Plant Science*, **15**, 1355941.
- Al Husaini M., Raharja A.R., Cahaya Putra V.H., Lukmana H.H., 2025. Enhanced plant disease detection using computer vision YOLOv11: Pre-trained neural network model application. *Journal of Computer Networks, Architecture and High Performance Computing*, **7**, 82–95.
- Brucal S. G. E., de Jesus L.C. M., Samaniego L.A., 2024. Development of a localized tomato leaf disease detection using YOLOv9 model via RoboFlow 3.0. In: *2024 IEEE 13th Global Conference on Consumer Electronics (GCCE)* (pp. 601–603).
- Banora M.Y., Voisin R., Nguyen V.C., Portier U., Bernabo C., Van Ghelder C., Lafargue, M., Tandonnet J.P., Demangeat G., Ollat N., Esmenjaud D., 2022. *Xiphinema index*-resistant grapevine materials derived from muscadine are also resistant to a population of *X. diversicaudatum*. *OENO One*, **56**, <https://doi.org/10.20870/oeno-one.2022.56.4.5791>.
- Çığsar I., Digiario M., Martelli G.P., 2002. Sanitary Status of Grapevine in South-Eastern and Central Anatolia (Turkey). *EPPO Bulletin*, **32**, 471-475.
- Demangeat G., Voisin R., Minot J.C., Bosselut N., Fuchs M., Esmenjaud D., 2005. Survival of *Xiphinema index* in vineyard soil and retention of Grapevine fanleaf virus over extended time in the absence of host plants. *Phytopathology*, **95**, 1151–1156.
- Fajardo T.V.M., Peres C.A., Nickel O., 2023. Real-time RT-PCR high-resolution melting curve analysis to detect and differentiate Brazilian variants of grapevine viruses. *Ciência e Técnica Vitivinícola*, **38**(2), 188-195.
- Gambino G., Gribaudo I., 2006. Simultaneous detection of nine grapevine viruses by multiplex reverse transcription-polymerase chain reaction with coamplification of a plant RNA as internal control. *Phytopathology*, **96**(11), 1223-1229.
- Gao L., Cao H., Zou H., Wu H., 2025. DMN-YOLO: A robust YOLOv11 model for detecting apple leaf diseases in complex field conditions. *Agriculture*, **15**, 1138.
- Gheorghe C., Duguleana M., Boboc R.G., Postelnicu C.C., 2024. Analyzing real-time object detection with YOLO algorithm in automotive applications: A review. *Computer Modeling in Engineering & Sciences*, **141**(3), 1939–1981.
- Ghafar A., Chen C., Shah S.A.A., Ur Rehman Z., Rahman G., 2024. Visualizing plant disease distribution and evaluating model performance for deep learning classification with YOLOv8. *Pathogens*, **13**(12), 1032.
- Jackson R.S., 2014. Vineyard practice. In *Wine science* (pp. 143–306). Elsevier.
- Jafar A., Bibi N., Naqvi R.A., Sadeghi-Niaraki A., Jeong D., 2024. Revolutionizing agriculture with artificial intelligence: Plant disease detection methods, applications, and their limitations. *Frontiers in Plant Science*, **15**, 1356260.
- Khanam R., Hussain M., Hill R., Allen P., 2024. A comprehensive review of convolutional neural networks for defect detection in industrial applications. *IEEE*, **12**, 94250–94295.
- Lee Y.S., Patil M.P., Kim J.G., Seo Y.B., Ahn D.H., Kim G.D., 2025. Hyperparameter optimization for tomato leaf disease recognition based on YOLOv11m. *Plants*, **14**(5), 653.
- Liu Y., Yu Q., Geng S., 2024. Real-time and lightweight detection of grape diseases based on Fusion Transformer YOLO. *Frontiers in Plant Science*, **15**, 1269423.
- Maroun R.G., Rajha H.N., Vorobiev E., Louka N., 2017. Emerging technologies for the recovery of valuable compound from grape processing by-products. In: C. M. Galanakis (Ed.), *Handbook of grape processing by-products: Sustainable solutions* (pp. 55–89). Academic Press.
- Medojević S., 2024. Potato leaf disease detection using Faster R-CNN and YOLO models. *International Journal of Multidisciplinary Studies and Innovative Technologies*, **8**(2), 144–150.
- Mora J.J., Blomme G., Safari N., et al., 2025. Digital framework for georeferenced multiplatform surveillance of banana wilt using human-in-the-loop AI and YOLO foundation models. *Scientific Reports*, **15**, 3491.
- M'rabet Samaali B., Mougou Hamdane A., Toumi A., Dhaouadi S., Kallel S., 2022. Transmission and translocation of Grapevine fanleaf virus (GFLV) from *Vitis vinifera* L. pollen to seeds and grape. *Archives of Phytopathology and Plant Protection*, **55**, 2040–2056.
- Öztürk L., Avcı G.G., Behmand T., Elekcioglu H.I., 2017. Incidence of viruses and vector nematodes in Thrace vineyards, Turkey. *International Journal of Agriculture and Environmental Research*, **3**(6), 4078-4089.
- Qi Z., Wang J., 2025. PMDNet: An improved object detection model for wheat field weed. *Agronomy*, **15**(1), 55.
- Patel S., Patel D., Patel A., Nanavati J., Patel U., Faldu A., Shingala A., 2024. Accurate and Efficient Real-Time Crop and Weed Identification Using YOLO-NAS: A Neural Architecture Search-Optimized Object Detection Model. *International Journal of Engineering Trends and Technology*, **72**(10), 35-45.
- Rahman S.U., Alam F., Ahmad N., Arshad S., 2023. Image processing-based system for the detection, identification and treatment of tomato leaf diseases. *Multimedia Tools and Applications*, **82**, 9431–9445.

- Raski D.J., Hewitt W.B., 1960. Experiments with *Xiphinema index* as a vector of fanleaf of grapevines. *Nematologica*, **5**, 166–170.
- Raski D.J., Hewitt W.B., Goheen A.C., Taylor C.E., Taylor R.H., 1965. Survival of *Xiphinema index* and reservoirs of fanleaf virus in fallowed vineyard soil. *Nematologica*, **11**, 349–352.
- Redmon J., Divvala S., Girshick R., Farhadi A., 2016. You only look once: Unified, real-time object detection. In: 2016 *IEEE Conference on Computer Vision and Pattern Recognition (CVPR)* (pp. 779–788).
- Rowhani A., Chay C., Golino D.A., Folk B. W., 1993. Development of a polymerase chain reaction technique for the detection of Grapevine fanleaf virus in grapevine tissue. *Phytopathology*, **83**(7), 749–753.
- Sapkota R., Flores-Calero M., Qureshi R., Badgajar C., Nepal, U., Poulouse A., Zeno P., Vaddevolu U.B.P., Khan S., Shoman M., Yan H., 2025. YOLO advances to its genesis: A decadal and comprehensive review of the You Only Look Once (YOLO) series. *Artificial Intelligence Review*, **58**(9), p.274.
- Singh V., Misra A.K., 2017. Detection of plant leaf diseases using image segmentation and soft computing techniques. *Information Processing in Agriculture*, **4**(1), 41–49.
- Slimani H., El Mhamdi J., Jilbab A., 2023. Artificial intelligence-based detection of fava bean rust disease in agricultural settings: an innovative approach. *International Journal of Advanced Computer Science and Applications*, **14**(6).
- Sonawane S., Patil, N.N., 2024. Comparative performance analysis of YOLO object detection algorithms for weed detection in agriculture. *Intelligent Decision Technologies*, **19**(1), 507–519.
- Tao J., Li X., He Y., Islam M.A., 2025. CEFW-YOLO: A high-precision model for plant leaf disease detection in natural environments. *Agriculture*, **15**(8), 833.
- Taylor C.E., Raski D.J., 1964. On the transmission of Grape fanleaf by *Xiphinema index*. *Nematologica*, **10**, 486–495.
- Temrokov A.Z., Bzhikhatlov K. Ch., 2025. Intelligent recommendation system for apple orchard protection in the Kabardino-Balkarian Republic. *News of the Kabardino-Balkarian Scientific Center of RAS*, **27**(2), 23–36.
- Terven J., Córdova-Esparza D.M., Romero-González J.A., 2023. A comprehensive review of yolo architectures in computer vision: From YOLOv1 to YOLOv8 and YOLO-NAS. *Machine Learning and Knowledge Extraction*, **5**(4), 1680-1716.
- Tian Y., Ye Q., Doermann D., 2025. Yolov12: Attention-centric real-time object detectors. *arXiv preprint arXiv:2502.12524*.
- Tripathi A., Gohokar V., Kute R., 2024. Comparative analysis of YOLOv8 and YOLOv9 models for real-time plant disease detection in hydroponics. *Engineering, Technology & Applied Science Research*, **14**(5), 17269–17275.
- Wang H., Zhang Y., Zhu C., 2025. DAFPN-YOLO: An improved UAV-based object detection algorithm based on YOLOv8s. *Computers, Materials & Continua*, **83**(2), 1929–1949. <https://doi.org/10.32604/cmc.2025.061363>.
- Wang C., Wang L., Ma G., Zhu L., 2025. CSF-YOLO: A lightweight model for detecting grape leafhopper damage levels. *Agronomy*, **15**(3), 741.
- Van Zyl S., Vivier M.A., Walker M.A., 2012. *Xiphinema index* and its relationship to grapevines: A review. *South African Journal of Enology and Viticulture*, **33**(1), 21–32.
- Zhu J., Qiu J., Chen S., Chen S., Zhang H., 2025. An application of YOLOv8 integrated with attention mechanisms for detection of grape leaf black rot spots. *PLoS ONE*, **20**(4), e0321788.